Problems Associated With the Direct Torque Control of an Interior Permanent-Magnet Synchronous Motor Drive and Their Remedies

Muhammed Fazlur Rahman, *Senior Member, IEEE*, Md. Enamul Haque, *Member, IEEE*, Lixin Tang, *Student Member, IEEE*, and Limin Zhong

***Abstract*—This paper investigates problems associated with the implementation of a direct torque control (DTC) strategy for an interior permanent-magnet synchronous motor drive. The DTC technique is increasingly drawing attention because of elimination of current controllers and, hence, their inherent delays, and elimination of the rotor position sensor. The latter advantage perhaps is the main impetus for considering this new approach of torque control. Problems associated with this controller, namely, the offset in the current measurements, the stator resistance variation, and the requirement of initial rotor position are addressed in this paper. Ways of mitigating of these problems are also investigated in this paper. These are evaluated with modeling and experimental studies, results of which are also presented.**

***Index Terms*—Parameter estimation, permanent-magnet motors, position measurement, torque control.**

I. Introduction

ALTHOUGH direct torque control (DTC) has some attractive features such as lesser parameter dependence, fast dynamic response, and no requirement for mechanical rotor position sensor for the inner torque control loop [1], [2], there exist some problems/limitations associated with this method of control, namely, 1) drift in stator flux linkage estimation due to offset error in measurement; 2) error in the estimation of stator flux linkage due to variation of stator resistance; and 3) requirement of a mechanical position sensor to detect the initial rotor position.

In a DTC scheme, the stator flux linkage is estimated by integrating difference between the input voltage and the voltage drop across the stator resistance given by (1).

$$\boldsymbol{\lambda}_s = \int_0^t (\boldsymbol{v}_s - R\boldsymbol{i}_s)dt + \boldsymbol{\lambda}_s|_{t=0} \tag{1}$$

where $\boldsymbol{\lambda}_s|_{t=0}$ is the initial stator flux vector at $t = 0$, and R and $\boldsymbol{v}_s$ are the stator resistance and the applied voltage vector, respectively. Because of the integration process, any dc offset in the measurements of $\boldsymbol{v}_s$ and $\boldsymbol{i}_s$ would eventually lead to large drifts in the computed (estimated) stator flux linkage. The integrator must be reset regularly to reduce the effect of the offset error. A few compensation techniques of this offset have been reported in the literature [3]–[6]. Chapuis *et al.* [3] proposed a method to eliminate the dc offset. However, a constant level of dc offset is assumed, which is often not the case. Low-pass filters (LPFs) have also been used/proposed to estimate the stator flux linkage [4]–[6]. In [4], a programmable cascaded LPF was proposed to replace the single-stage integrator for calculating the stator flux linkage, for application in stator flux orientation for an induction motor drive. The torque was still controlled via current control, however. Simulation results presented in [4] demonstrate the ability of the cascaded filter in calculating the stator flux linkage.

In this paper, this approach of [4] has been further investigated and implemented for compensation of offset error in a direct torque controlled interior permanent-magnet (IPM) synchronous motor drive. It is shown that programmable cascaded LPF can also be adopted to replace the integrator and compensate for the effect of dc offsets in a direct-torque-controlled IPM synchronous motor drive, thereby improving the performance of the drive.

Variation of stator resistance also introduces error in stator flux estimation, especially at low speed. The voltage drop in stator resistance at low speeds is relatively large and may become comparable to the back electromotive force (EMF). If the stator resistance value deviates from the one used in the estimator (1), large errors between the reference and actual stator flux linkage vector and torque occurs and the drive easily becomes unstable when operating speed is low and load is high. A number of researchers have recently addressed the issue of stator resistance variation issue for the induction machine. For example, Mir *et al.* [7] has contributed a thorough work on an induction machine. They proposed fuzzy and proportional–integral (PI) stator resistance estimators for a DTC induction machine drive system and compared the two estimators. The estimation of stator resistance is based on the error between the reference current and the actual current. However, they did not give details of how to obtain the reference current for the stator resistance estimator. Some stability problems of the fuzzy estimator were observed when torque reference value was small. A stator resistance observer based on fuzzy logic for induction motor was reported in [8]. Although it is a *de facto* open-loop controller based on fuzzy rules, acceptable accuracy (5%) of stator resistance estimation has been achieved. However, this

Manuscript received April 30, 2003; revised October 27, 2003. Abstract published on the Internet May 20, 2004.

M. F. Rahman and L. Tang are with the School of Electrical Engineering and Telecommunications, The University of New South Wales, Sydney, NSW 2052, Australia (e-mail: f.rahman@unsw.edu.au; lixin.tang@ieee.org).

M. E. Haque is with the Department of Electrical Engineering, King Saud University, Riyadh 11421, Saudi Arabia (e-mail: enamul@ksu.edu.sa).

L. Zhong is with Cochlear Limited, Lane Cove, NSW 2066, Australia (e-mail: lzhong@cochlear.com.au).

Digital Object Identifier 10.1109/TIE.2004.831728

fuzzy estimator needs many rules, which are based on extensive experiments and therefore, it is not easy to implement. Lee and Krishnan [9] also developed a PI resistance estimator for a DTC induction motor drive. They also presented the mathematical relationships between stator current, torque command, flux command, and machine parameters. They also analyzed the instability caused by the estimation error in stator resistance.

For the IPM DTC drives, the same issue of stator resistance variation remains. A PI stator resistance estimator based on the error in flux linkage [10] was reported by the authors of this paper for the IPM machine. It is based on the notion that the variation of the stator resistance of the PM machine will cause a change in the amplitude of the actual flux linkage. A simple PI controller tracks the stator resistance by eliminating the error in the command and actual flux linkage, by running parallel to the hysteresis flux controller for the DTC. However, the rotor position needed to be known in order to obtain the actual flux linkage. In this paper, a new PI stator resistance estimator is presented, which can track variation of stator resistance without requiring any position information.

The direct torque control algorithm described in Section II requires the initial position of the rotor at power-on. Without knowing the initial rotor position, $\boldsymbol{\lambda_s}|_{t=0}$ in (1) estimation of stator flux linkage cannot proceed well. To successfully start the motor under DTC from any position, the initial position must also be known. Since the DTC scheme of Section II does not explicitly require the rotor position continuously, an initial position estimator without a mechanical position sensor is required.

A number of procedures [11]–[22] have been suggested recently for the detection of the initial rotor position at standstill for different types of PM motors. These methods are based on the following schemes:

- Kalman filters and state observers;
- voltage/current harmonic measurement;
- introduction magnetic saliency;
- application of voltage pulses;
- injection of current signal.

These approaches for position estimation of IPM synchronous motor have one or more of the following limitations.

- Most of the methods fail at standstill since the rotor magnet does not induce any voltage and, therefore, no information of the magnetization is available.
- Position estimation is load dependent.
- There are excessive computation and hardware requirements.
- There is the need of one or more pulsewidth-modulation (PWM) current controllers, which are not required for a DTC controller.

Recently, it has been demonstrated that rotor position can be estimated by applying high-frequency voltage to the motor [20]–[22]. The present generation of inverters with fast switches makes this approach easily applicable. It has been found that this approach can also be adopted for a DTC controlled IPM synchronous motor drive to obtain the initial position of the rotor. The initial rotor position can be estimated by applying a three-phase high-frequency sinusoidal voltage to the motor and analyzing the effect of the saliency on the amplitude of the corresponding stator current. The magnetic polarity of the initial position is also identified by using the relative amplitudes of stator currents that occur as a result of increased or decreased magnetization according to the polarity of the rotor at the initial position.

The above-mentioned problems must be minimized or removed to enhance the performance of the DTC IPM drive. In this paper, mitigation techniques for these problems are investigated through modeling and experimental evaluation. These results are presented.

II. The DTC Scheme and its Model

The basic principle of DTC is to select stator voltage vectors according to the differences between the reference and actual torque and flux linkage. Current controllers followed by pulsewidth modulators are not used in a DTC system, and the parameters of the motor are also not used, except for the stator resistance. Therefore, the DTC possesses advantages, such as lesser parameter dependence and fast torque response when compared with the torque control via PWM current control. Figs. 1 and 2 show the schematic of the basic DTC controller, and its switching vectors, respectively. Torque and stator flux linkage are controlled using two hysteresis comparators which operate independently of each other. The outputs of these controllers apply appropriate voltage vectors via the inverter in a way to force the two variables to predefined trajectories. Switching states of the inverter, the dc-link voltage (sensed) of the inverter and two of the motor currents (sensed) can be used to obtain the stator voltage and current vectors of the motor in the stator DQ frame.

The D- and Q-axes stator flux linkages, λ_D and λ_Q in the stationary reference frame, are then given by

$$\lambda_{D(k)} = \lambda_{D(k-1)} + \{v_{D(k-1)} - R\bar{i}_{D(k)}\}T_s \tag{2}$$

$$\lambda_{Q(k)} = \lambda_{Q(k-1)} + \{v_{Q(k-1)} - R\bar{i}_{Q(k)}\}T_s \tag{3}$$

where $\bar{i}_{D(k)} = (i_{D(k-1)} + i_{D(k)}/2)$, $\bar{i}_{Q(k)} = (i_{Q(k-1)} + i_{Q(k)}/2)$, T_s is the sampling interval, v_D, v_Q are the stator voltages in the D and Q axes, i_D, i_Q are the stator currents in the D and Q axes, and variables k and $k-1$ in brackets refer to the k th and $k-1$ th sampling instants, respectively. The stator flux linkage vector is then given by

$$\boldsymbol{\lambda}_{s(k)} = \sqrt{\lambda_{D(k)}^2 + \lambda_{Q(k)}^2}\angle \tan^{-1}\left(\frac{\lambda_{Q(k)}}{\lambda_{D(k)}}\right) = \hat{\lambda}_{s(k)}\angle\lambda_{s(k)}. \tag{4}$$

The motor developed torque in terms of the stator flux linkages is given by

$$T(k) = \frac{3}{2}P\left\{\lambda_{D(k)}i_{Q(k)} - \lambda_{Q(k)}i_D(k)\right\} \tag{5}$$

where P is the number of pole pairs. The motor developed torque, in terms of the stator and rotor flux linkage amplitudes, is also given by

$$T(k) = \frac{3P\hat{\lambda}_{s(k)}}{4L_dL_q}\Big[2\lambda_f L_q \sin\{\delta(\kappa)\} - \hat{\lambda}_{s(k)}(L_q - L_d)\sin 2\{\delta(\kappa)\}\Big] \tag{6}$$

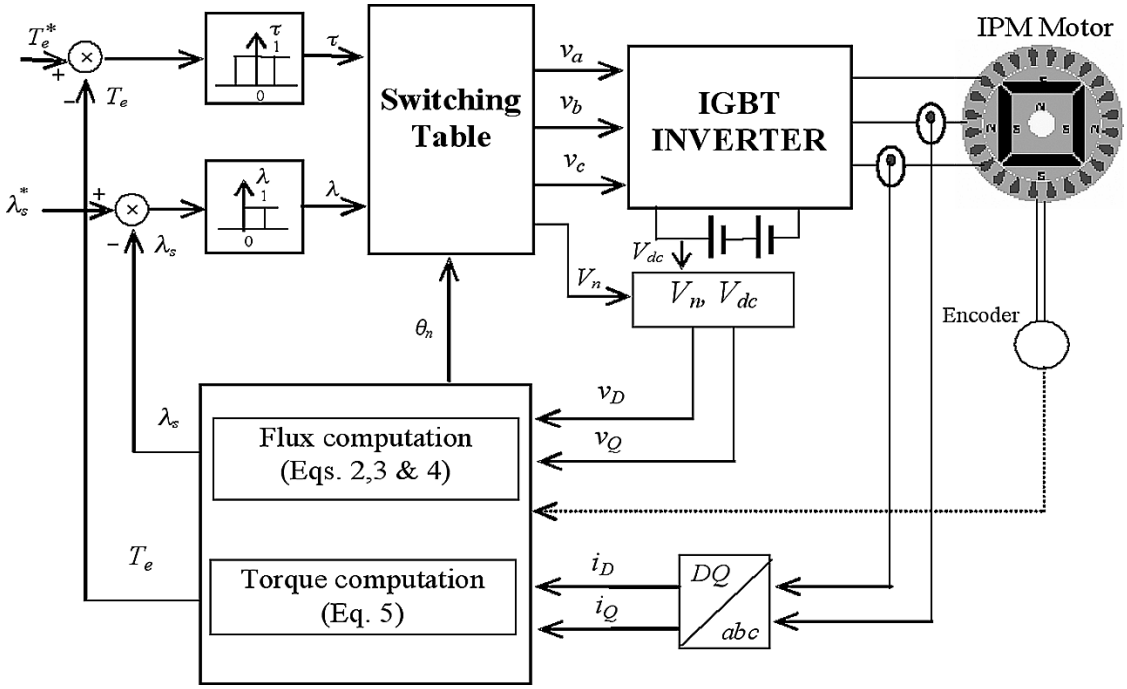

Fig. 1. The DTC scheme.

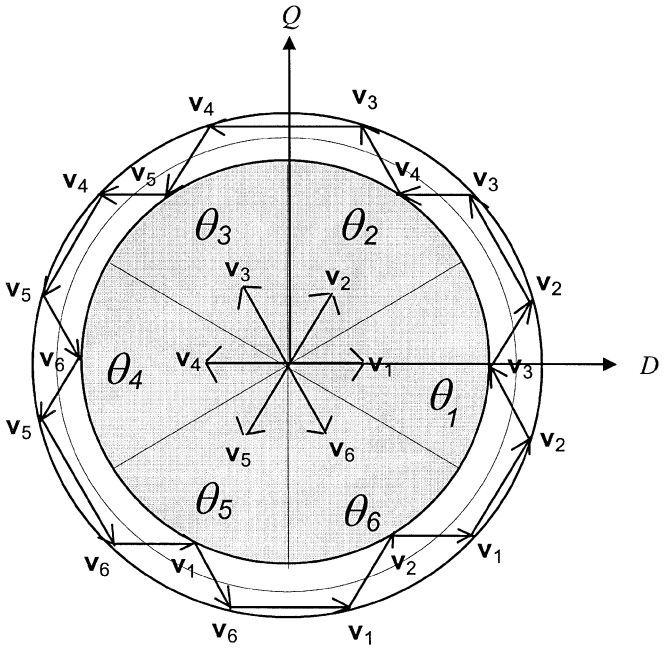

Fig. 2. Switching vectors for DTC.

where λ_f is the stator flux linkage due to the rotor PM excitation only. Equations (4)–(6) are needed to implement the DTC controller of Fig. 4(a). A full description of the DTC scheme for the IPM synchronous motor is available in [1] and [2] and will not be repeated here.

III. Effect of the Offset Error and its Remedy

A. Effect of Offset Error

Offsets in measurements of the dc-link voltage and currents are inevitable. These are inherent in the sensors and the signal conditioning circuits used. These offsets are dc signals and their magnitudes also depend on temperature. The integration process in (1) will integrate these errors and unless reset, they will grow to large values leading to instability. Fig. 4(a) indicates estimated stator flux linkages (experimental results) when dc offsets are present. Torque developed by the motor (described in Table I) oscillates at the stator electrical frequency, which causes ripples in speed as shown in Fig. 4(b).

TABLE I
Parameters of IPM Motor Used

Number of pole pairs	P	2
Stator resistance	R	19.4 Ω
Magnet flux linkage	λ_f	0.447 Wb
d-axis inductance	L_d	0.3885 H
q-axis inductance	L_q	0.4755 H
Phase voltage	V	240 V
Phase current	I	1.4 A
Base speed	ω_b	1500 rpm

B. Compensation for Offset Error

It is observed that offset errors result in a drift of stator flux linkage locus [Fig. 4(a)]. A programmable cascaded LPF can be used to compensate for the offset error. The transfer characteristic of an LPF is

$$\frac{Y}{X} = \frac{1}{1 + j\tau\omega} \tag{7}$$

where τ is the filter time constant and ω is the frequency of the signal. The phase lag and the gain of the filter can be given by

$$\phi = \tan^{-1}(\tau\omega) \tag{8}$$

$$K = \frac{1}{\sqrt{1 + (\tau\omega)^2}} \tag{9}$$

where ϕ is the phase lag and K is the gain. If n number of filters are cascaded, the total phase lag and the gain are given as

$$\phi_T = \phi_1 + \phi_2 + \cdots + \phi_n = \tan^{-1}(\tau_1\omega) + \tan^{-1}(\tau_2\omega) + \cdots + \tan^{-1}(\tau_n\omega) \quad (10)$$

$$K_T = K_1 K_2 \ldots K_3. \quad (11)$$

If all filters are identical, that is, all have the same time constant τ and gain K, (10) and (11) become

$$\phi_T = n\phi = n\tan^{-1}(\tau\omega) \quad (12)$$

$$K_T = K^n = \frac{1}{\left(\sqrt{[1+(\tau\omega)^2}\right)^n}. \quad (13)$$

It is known that the phase lag and gain of a pure integrator for a sinusoidal signal are 90° and $1/\omega$ respectively, where ω is the angular frequency of the signal. If the programmable cascaded LPF is to perform the function of an integrator, it must satisfy the following two conditions:

$$\phi_T = 90^o \quad (14)$$

$$GK_T = \frac{1}{\omega} \quad (15)$$

where G is the gain needed for compensation. Substituting (12) and (13) into (14) and (15) gives

$$\tau = \frac{\tan\left(\frac{90^o}{n}\right)}{\omega} \quad (16)$$

$$G = \frac{\left(\sqrt{[1+(\tau\omega)^2]}\right)^n}{\omega}. \quad (17)$$

Equations (16) and (17) give the parameters τ and G as functions of frequency, or the rotor speed, at a steady speed. If the signal has a dc offset, the filter can always perform the task of integration by programming τ and G. When the signal is dc, τ and G become infinite and the filter therefore can not perform the integration.

To realize the filter in software, the transfer characteristic of the filter has to be expressed in discrete form. The discrete transfer characteristic of an LPF is

$$\frac{Y}{X} = \frac{1}{1+\tau\frac{1-z^{-1}}{T_s}} = \frac{T_s}{T_s+\tau(1-z^{-1})} \quad (18)$$

where T_s is the sampling time and τ is the time constant. The corresponding difference equation is

$$y(kT_s) = \frac{1}{T_s+\tau}\left[T_s x(kT_s) + \tau y(kT_s - T_s)\right]. \quad (19)$$

Fig. 3 shows the block diagram of the three-stage programmable cascaded LPF. For three identical LPFs connected as shown in Fig. 3, n is equal to 3 and τ and G can be accordingly determined.

Fig. 4(a) and (b) shows the locus of the stator flux and speed without compensation for the offset error. The drift in the flux linkage from the origin which is the ideal location and the ripple in speed are evident. Fig. 4(c) and (d) shows the stator flux locus and speed, when the integrator is reset by the cascaded LPF as described earlier. The flux locus now remains centered on the origin and the ripple in speed has been significantly reduced. The usefulness of the three-stage cascaded LPF is clearly demonstrated.

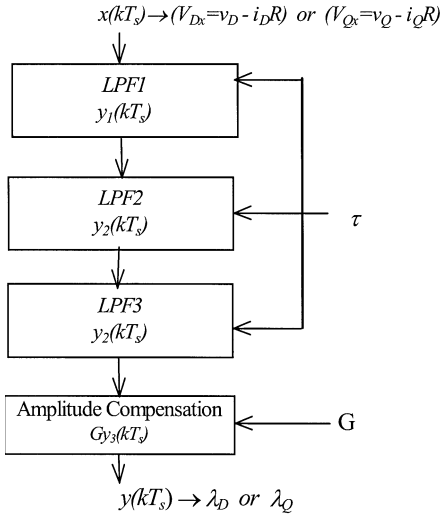

Fig. 3. Block diagram of a three-stage programmable cascaded LPF.

IV. Effect of Stator Resistance Variation and Its Compensation

A. Effect of Stator Resistance Variation

As mentioned earlier, the stator flux vector is highly affected by the change in stator resistance, particularly at low speed. The stator resistance changes due to the change in temperature during the operation of the machine because of the stator copper and other machine losses. The copper loss, which dominates the other losses, relates to the stator current. The variation of the stator resistance is a thermal process, and therefore a function of time. The stator resistance may change by about 1.5–1.7 times of its nominal value [9]. For the motor under test (Table I), 55% increase in R for full-load operation at 200 r/min was noted. The drive system may become unstable if the stator resistance value used in the controller differs from that of the actual machine resistance. Fig. 5 shows modeling results when the stator resistance is increased by 30%, and the controller uses the nominal R. The mismatch between the resistance in the controller and the motor causes the actual flux locus to deviate from the ideal circle of Fig. 5(a) as indicated in Fig. 5(b). This causes oscillations in motor torque and speed.

B. Compensation for Stator Resistance Variation

Performance of the DTC drive can be enhanced if the stator resistance is continuously estimated and updated in the controller during operation of machine. It is seen that if an error in stator resistance between the controller and the motor is present, there will be errors in the estimated flux linkage and torque. The estimated torque is larger than the actual torque when the actual stator resistance is larger than the resistance in the controller and

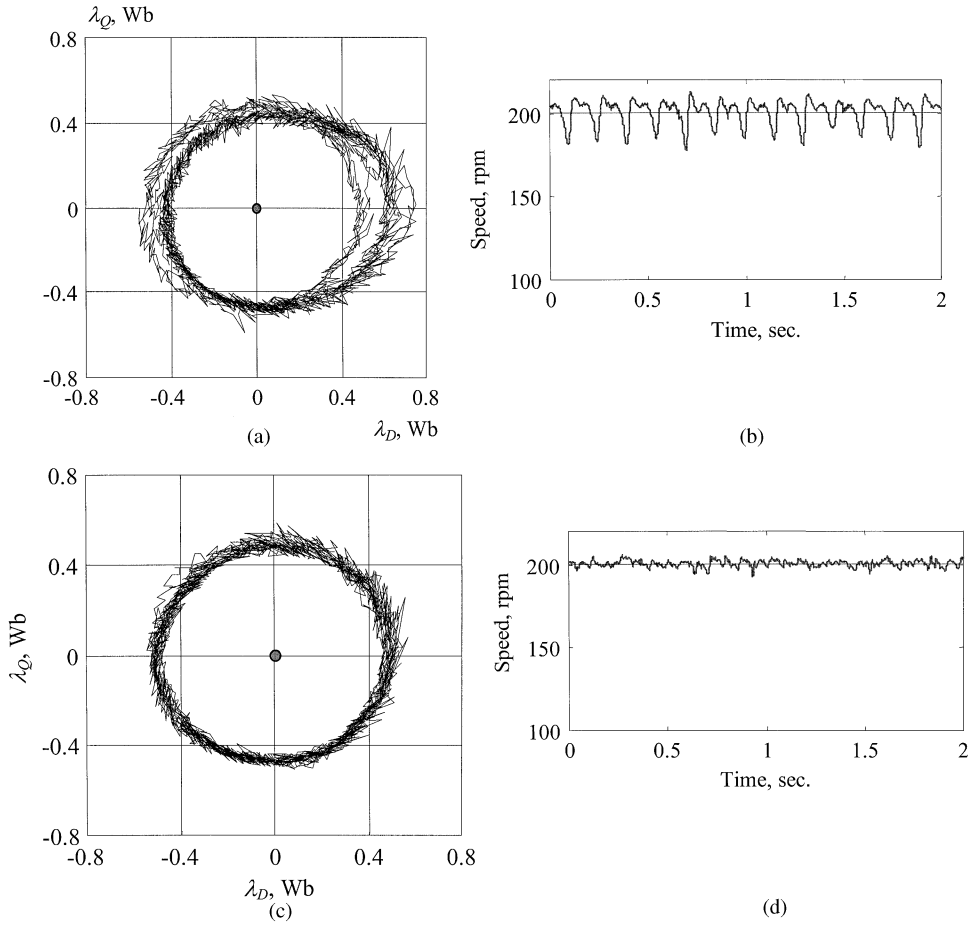

Fig. 4. Effects of offset error on stator flux linkage and motor speed. (a), (b) Without compensation. (c), (d) With compensation.

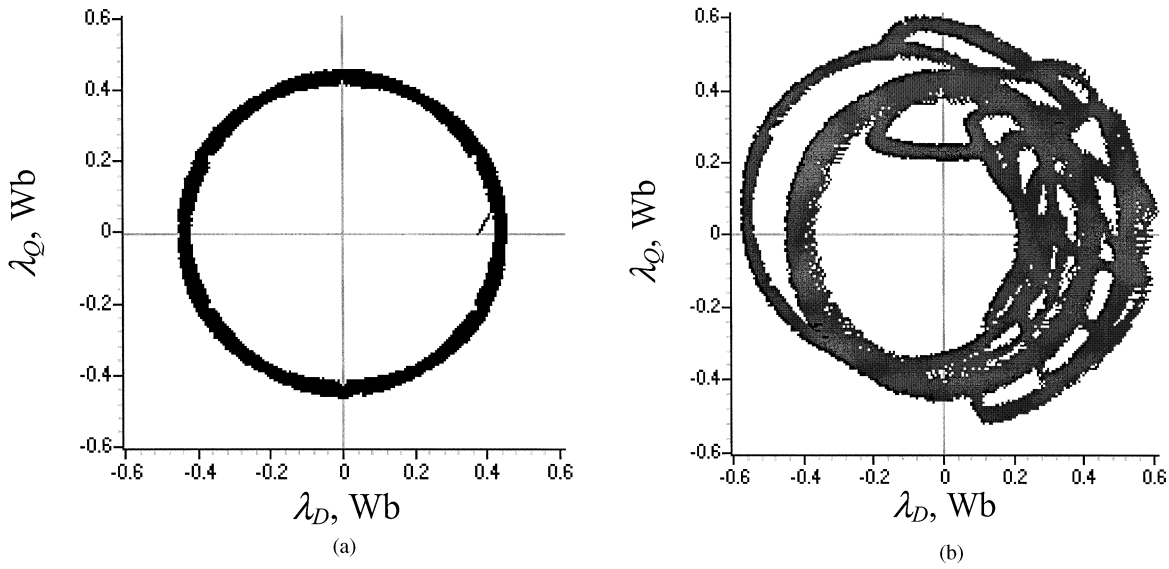

Fig. 5. Flux locus variation with (a) nominal, (b) 30% increased, stator resistance.

vice versa. This will reduce the maximum output torque of the drive. It should be also noted that the amplitude of the current is different from its value if the two resistances did not differ. Because the stator current is measured, it should be possible to use the stator current to track the change in stator resistance.

Based on the relationship between change of resistance and change of current, a PI stator resistance estimator (SRE) can be constructed as indicated in Fig. 6, where change in stator resistance ΔR is given by

$$\Delta R = \left(k_p + \frac{k_i}{s}\right) \Delta I. \tag{20}$$

The compensation process can be based on the premise that as stator resistance changes, so will the amplitude of the stator

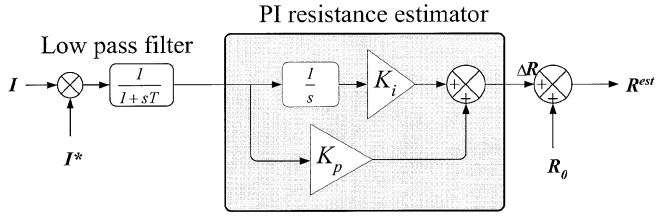

Fig. 6. Block diagram of a PI stator resistance estimator.

current vector. The error between the amplitude of the measured current vector and that of the reference current vector can be used to compensate for the change in stator resistance until the error in current becomes zero in the steady state. This zero error is forced by the integrator in the estimator.

The reference current vector can be derived from the reference torque and reference flux as shown below. The IPM machine's torque and flux vector can be described by (21) in the rotor reference frame

$$\begin{cases} T^* = \frac{3P}{2}[\lambda_f i_q - (L_q - L_d) i_d i_q] \\ \lambda^* = \sqrt{(L_d i_d + \lambda_f)^2 + L_q^2 i_q^2} \end{cases} \tag{21}$$

$$I^* = \sqrt{i_d^2 + i_q^2}. \tag{22}$$

It is seen that i_d and i_q corresponding to different reference flux linkage and torque values can be obtained by solving (21). The amplitude of the current vector can be calculated by (22). It should also be noted that there is no stator resistance term in (21); therefore, the solution should always be independent of stator resistance.

The curves representing (21) at different flux and torque values are shown in Fig. 7(a). The solid curves represent currents for a few torque values and the dotted curves represent currents for a few flux linkage values. The intersection points represent the solutions to (21) in the i_d-i_q plane in the rotor reference frame. The distance from the cross points to the origin is the amplitude of the reference current. After solving (21), i_d and i_q can be obtained, therefore, the amplitude of the current vector can be calculated from (22). A map of the reference currents at different reference torque and flux linkage values is shown in Fig. 7(b). For real-time application, a lookup table of reference current at different reference flux linkage and torque values can be formed to save the execution time. The variation of the stator resistance will not affect this lookup table. Therefore, it is possible to use it to compensate for any resistance variation. Although all the equations are in the rotor frame, it should be noted that the amplitude of the current vector is independent of reference frame. Therefore, rotor position is not necessary for this PI resistance estimator.

In order to validate the PI estimator for its ability to track the stator resistance variation, modeling work was carried out in which the stator resistance ramps up and down at a reasonable rate. The results are presented in Fig. 8(a). Although there is a delay for the estimator, the steady-state error of the stator resistance estimator is seen to reduce to zero. Therefore, the error in estimated flux linkage and torque due to stator resistance variation can be reduced to zero, also. As a result, the PI stator resistance estimator (PI-SRE) based on current amplitude scheme will improve the performance of the DTC drive by compensating for the variation of stator resistance.

Experimental work was also carried for the PI-SRE which was implemented for the DTC drive of the motor in Table I. Results from these tests are presented in Fig. 8(b). The top subplot shows the actual and the estimated stator resistances. A change of the actual stator resistance is introduced by switching in an extra resistance in each phase in the stator circuit. It is seen that the PI-SRE can reach the actual value of the stator resistance within a short time. The middle subplot is the amplitude of the current vector during this process. It is seen that the inrush current is eventually eliminated by the estimator. The amplitude of the current vector at the end is almost the same as that of the beginning. The bottom subplot shows the estimated torque in the duration. The estimated torque goes back to its original value when the actual resistance is estimated correctly. It should be noted that in practice, the stator resistance changes slowly, so that tracking is more accurate at all times than what is indicated in Fig. 8(b) for which an abrupt change of stator resistance was introduced. Clearly, the performance of the DTC drive is improved with this estimator.

V. Detection of Initial Rotor Position Without Position Sensor

The integration process in (1), which runs continuously, requires knowledge of the initial stator flux position $\lambda_{s|_{t=0}}$ at start. The stator current is assumed to be zero at start, so that the flux linkage due to the rotor only, i.e., λ_s at $t = 0$, must be known in order to start the motor without jitter. If the initial position information in the controller is inaccurate, the motor may initially rotate in the wrong direction. This dithering is unacceptable in applications such as disk drives, electric propulsion, and high-performance servos. Since the DTC scheme does not explicitly require the rotor position after start, an initial position estimator without any position sensor is desirable.

A sensorless method to estimate the initial rotor position has been investigated in this section. The method is based on the application of a high-frequency sinusoidal voltage and considering the effects of the saliency on the amplitude of the corresponding stator current component. The magnetic pole is identified using the effect of magnetic saturation. The method is suitable to be combined with a DTC drive. This method does not depend on the level of load or on any motor parameters.

In the proposed method a high-frequency ($f_h = 300$ Hz) sinusoidal voltage is applied to the stator of the IPM synchronous motor. At this frequency, the net torque developed by the stator currents I_h is negligible; hence, the rotor does not have to be held mechanically. The amplitude of the stator current I_h depends on the angular position of the rotor due to the saliency of the IPM motor and can be correlated with the angular position of the high frequency voltage phasor. This allows one to identify the initial rotor position of an IPM synchronous motor.

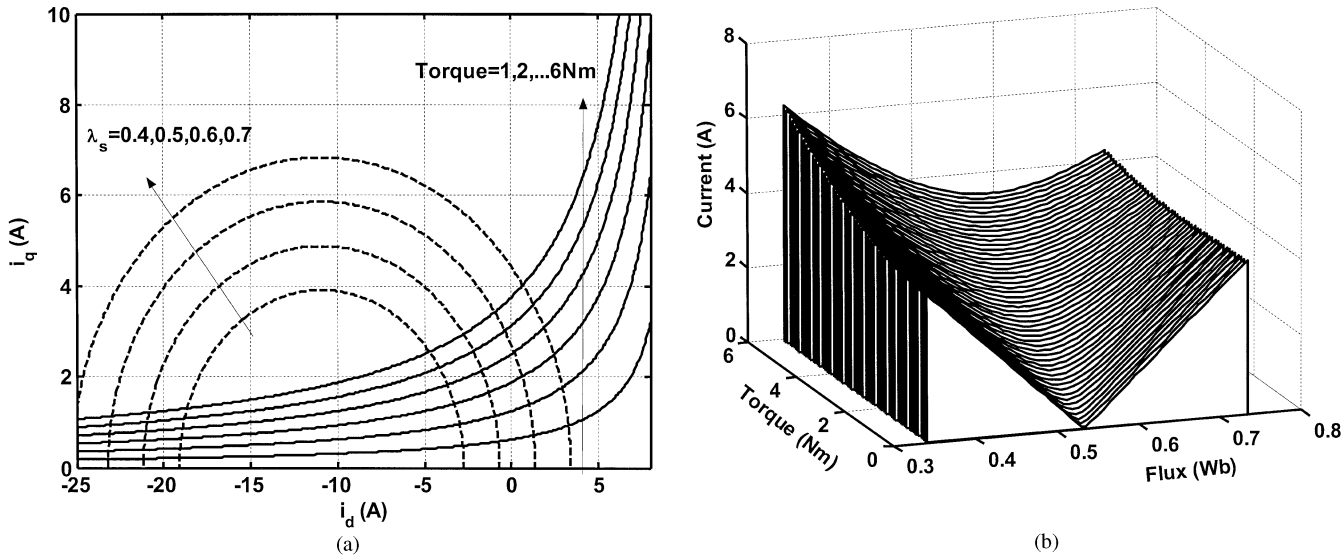

(a) (b)

Fig. 7. Curves representing (21) with different flux linkage and torque values and the amplitudes of the solutions.

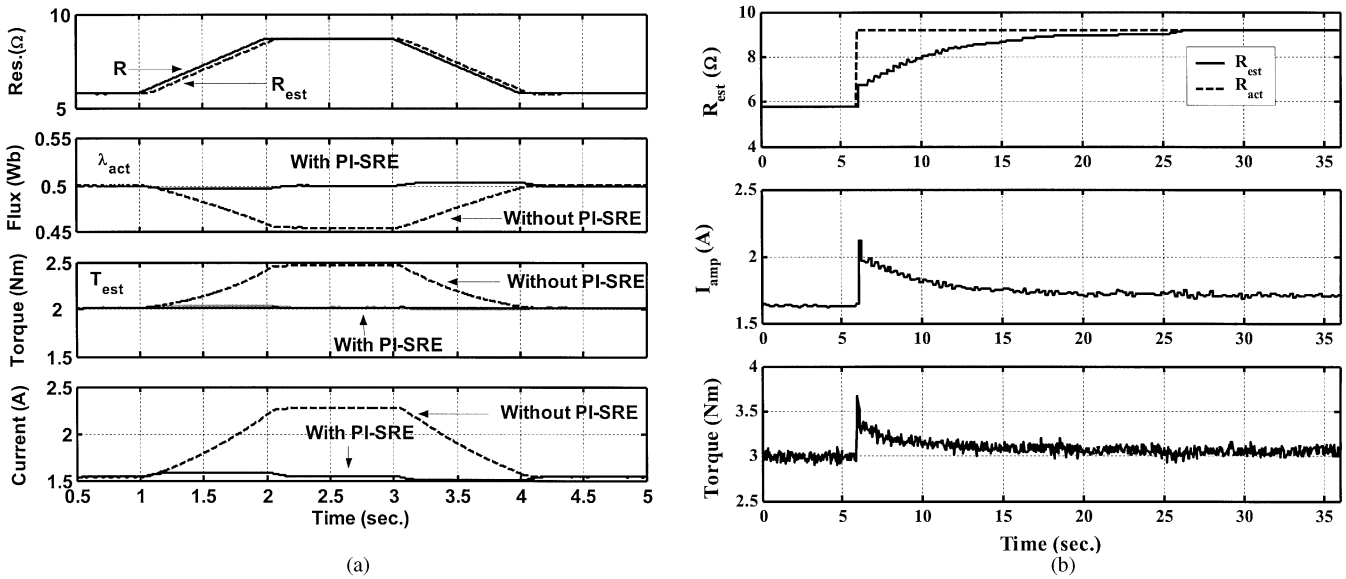

(a) (b)

Fig. 8. Modeling and experimental results of the stator resistance estimator.

Considering an IPM synchronous motor supplied only with the 300-Hz voltage component V_h, the mathematical model of IPM synchronous motor gives

$$\begin{aligned} V_{qh} &= V_h \sin\theta_h \\ &= Ri_{qh} + L_q \frac{di_{qh}}{dt} + \omega_r (L_d i_{dh} + \lambda_f) \qquad (23) \\ V_{dh} &= V_h \cos\theta_h \\ &= Ri_{dh} + L_d \frac{di_{dh}}{dt} - \omega_r L_q i_{qh} \qquad (24) \end{aligned}$$

where V_{qh} is the q-axis voltage component, V_{dh} is the d-axis voltage component, i_{qh} is the q-axis current component, i_{dh} is the $values$-axis current component, R is the stator resistance, L_d is the d-axis inductance, L_q is the q-axis inductance, λ_f is the magnet flux linkage, and

$$\theta_h = \int_0^t \omega_h dt + \theta_{h0}. \qquad (25)$$

The angle θ_h, expressed in electrical radians, is the angular position of the 300-Hz voltage vectors. Assuming zero rotor speed ($\omega_r = 0$) and $\theta_{h0} = 0$, solving (23) and (24) for i_{dh} and i_{qh}, the square of the current vector amplitude can be expressed as

$$\begin{aligned} I_h^2(t) &= i_{dh}^2 + i_{qh}^2 \\ &= f_1(t) + f_2(t) + f_3(t) \\ &= k_1 \cos^2\theta_h + k_2 \sin^2\theta_h + k_3 \sin 2\theta_h \qquad (26) \end{aligned}$$

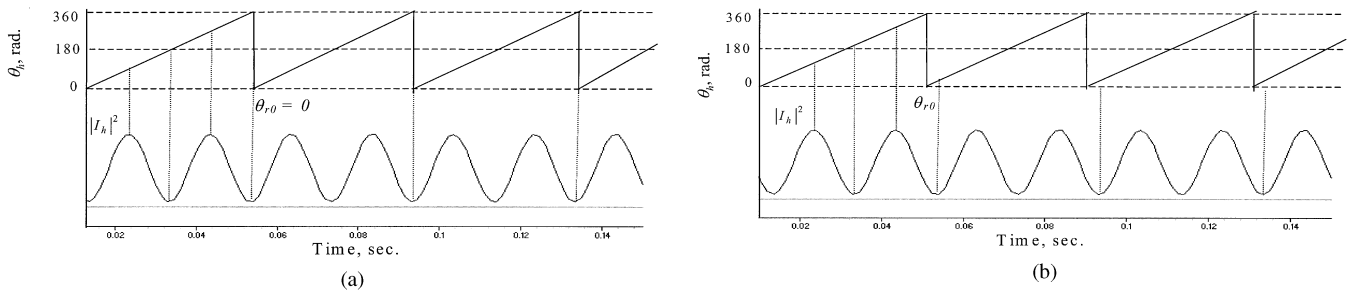

Fig. 9. Initial rotor-position estimation. Modeling results.

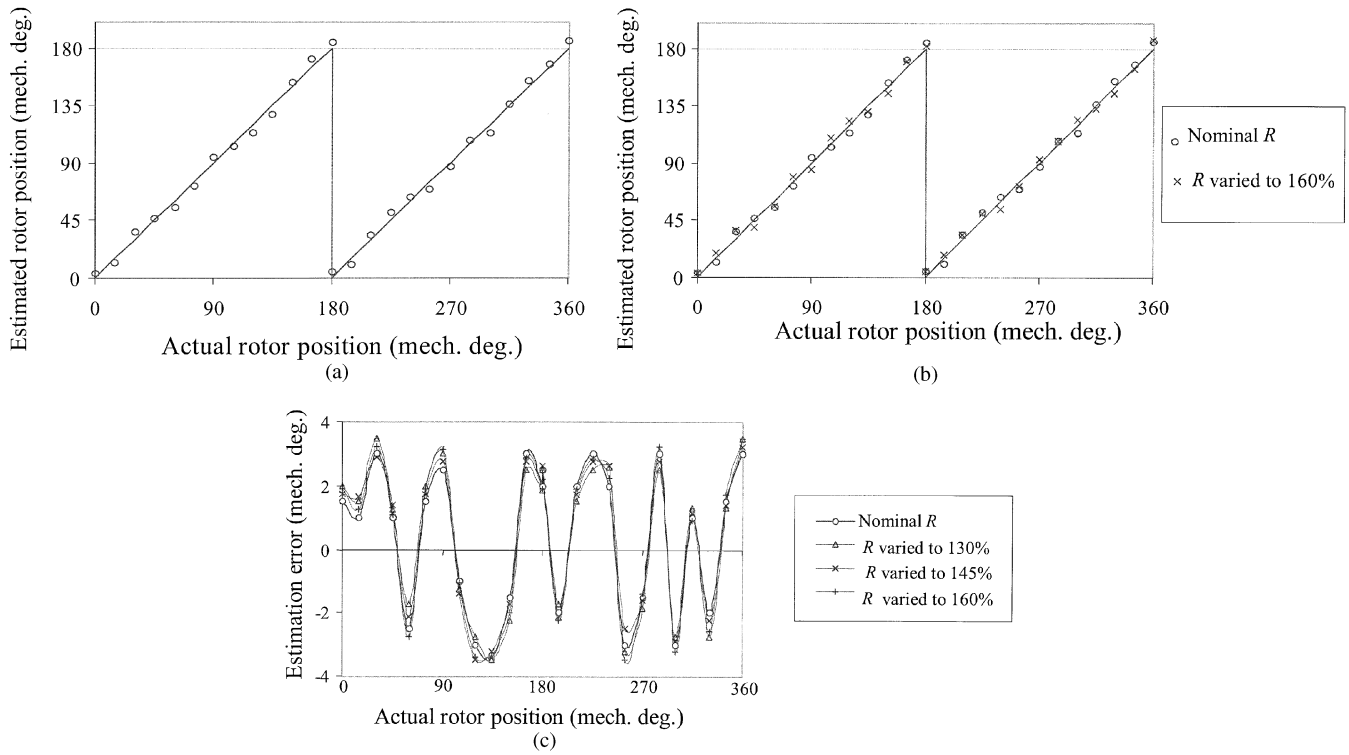

Fig. 10. Results of rotor-position estimation. Experimental result.

where

$$k_1 = V_h^2\left(\frac{R^2}{\left(R^2+\omega_h^2L_d^2\right)^2}+\frac{\omega_h^2L_q^2}{\left(R^2+\omega_h^2L_q^2\right)^2}\right)$$
$$k_2 = V_h^2\left(\frac{R^2}{\left(R^2+\omega_h^2L_q^2\right)^2}+\frac{\omega_h^2L_q^2}{\left(R^2+\omega_h^2L_d^2\right)^2}\right)$$
$$k_3 = V_h^2\left(\frac{R\omega_hL_d}{\left(R^2+\omega_h^2L_d^2\right)^2}+\frac{R\omega_hL_q}{\left(R^2+\omega_h^2L_q^2\right)^2}\right). \quad (27)$$

Substituting the parameters of an actual IPM synchronous motor as shown in Table I, it is possible to observe that at a sufficiently high f_h, the term $f_2(t)$ is largely dominant compared to $f_1(t)$ and $f_3(t)$, particularly at frequencies higher than 250 Hz [23].

At frequencies higher than 250 Hz, the contribution of the first and third terms can be neglected. Equation (26) can, thus, be reduced to

$$|I_h|^2 = f_2(t). \quad (28)$$

It can be observed that, for a four-pole machine with $\theta_{r0} = 0°$ [Fig. 9(a)], a minimum of $|I_h^2(t)|$ occurs when

$$\theta_h = k\pi, \qquad k = 0,1,2,\ldots \quad (29)$$

and a maximum occurs when

$$\theta_h = \frac{\pi}{2} + k\pi, \qquad (k = 0,1,2,\ldots \quad (30)$$

which means that a minimum of stator current amplitude occurs when the voltage vector is aligned with the minimum inductance axis and a maximum amplitude occurs when the voltage vector is aligned with the maximum inductance axis. From (28) and with $\theta_{r0} \neq 0°$ [Fig. 9(b)], a minimum of $I_h^2(t)$ occurs when

$$\theta_h = k\pi + \theta_{r0}, \qquad k = 0,1,2,\ldots \quad (31)$$

and a maximum of $I_h^2(t)$ occurs when

$$\theta_h = \frac{\pi}{2} + k\pi + \theta_{r0}, \qquad k = 0,1,2,\ldots. \quad (32)$$

This means that, at standstill, the position of the rotor can be simply measured as the angular displacement corresponding to

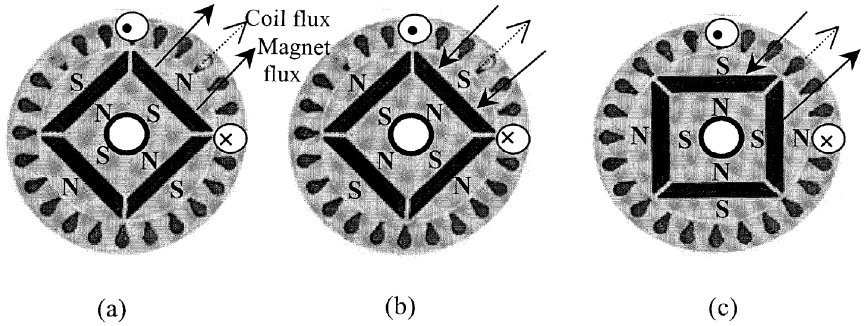

Fig. 11. Rotor flux affecting flux produced by stator coil.

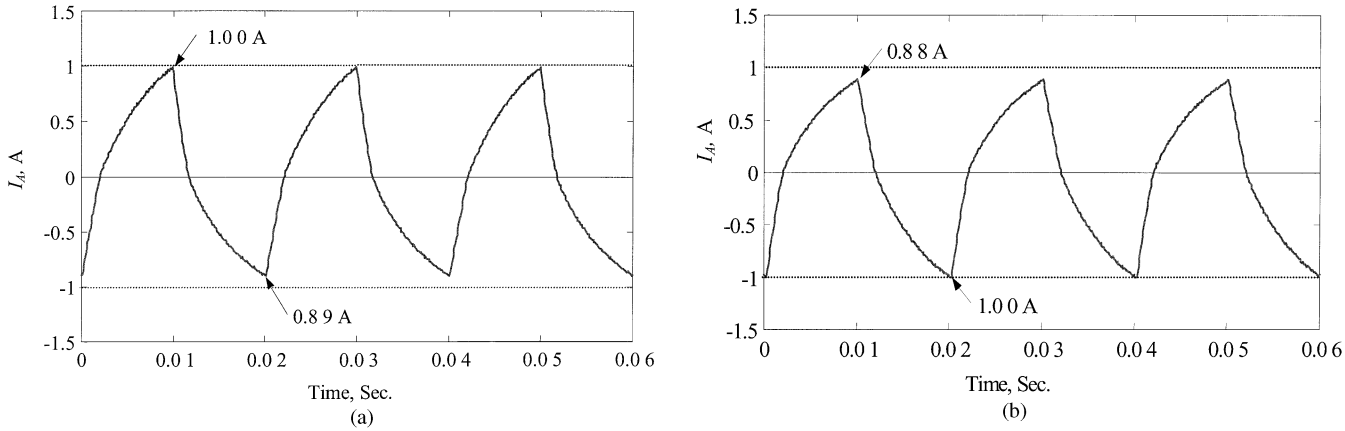

Fig. 12. Magnetic polarity detection with square-wave AC voltage. Experimental result.

the minimum and maximum values of $I_h^2(t)$ from (29)(32). This is also indicated in Fig. 9.

A. Results of Initial Rotor Position Detection Without Reference to Polarity of the Rotor

The experimental results of estimation are shown in Fig. 10, where the estimated rotor positions are plotted against the actual values of the rotor position over the mechanical angle from 0° to 360°. Experiments were performed with nominal R and with 130%, 145%, and 160% of the nominal value. It is observed from Fig. 12 that the estimated rotor position is very close to the actual initial rotor positions. Fig. 10(a) and (b) shows the experimental results over the range from 0° to 360° (mechanical) when the stator resistance is the nominal value and 145% of the nominal value, respectively. Fig. 10(c) shows the estimation error for a change of resistance value to 130%, 145%, and 160%. The error is found to be within the range of $-3.5°$ to $+3.5°$ (mechanical), which is quite acceptable for the DTC. It is seen from Fig. 10 that the estimated rotor position values exist only over the range 0° to 180° even though the actual rotor position exists over the range 0° to 360°. The polarity of the rotor position must be taken into account in order for the rotor position to be determined over the full 360°. The polarity discrimination is described in the following section.

B. Identification of Magnetic-Pole Orientation

The initial rotor position can be estimated with the procedure described above, but it has not yet been confirmed whether the estimated position corresponds to the north pole or south pole of the rotor magnets. A method to identify the polarity of the magnet is described in this section, which utilizes the magnetic saturation effect.

Fig. 11(a) shows a diagram of a four-pole IPM synchronous motor with one of the north poles aligned with the coil shown. Solid arrows represent the flux from the rotor magnet that links the coil. A dashed arrow represents the flux from current in the coil. Fig. 11(b) shows the rotor rotated to the position where one of the south poles is aligned with the coil. Fig. 11(c) shows the rotor rotated to a position where equal amounts of flux from north pole and south pole link the coil. When a north pole is aligned with the coil, the current in the coil increases the flux linked by the coil [Fig. 11(a)], increases stator saturation, and slightly decreases the inductance, which was present with no stator current. When a south pole is aligned with the coil, the current in the coil decreases the flux linked by the coil [Fig. 11(b)], decreases stator saturation and slightly increases the inductance that was present with no stator current. Since the inductance of the coil is different for north and south poles, the stator current will be different due to the variation of inductances.

A square-wave ac voltage can be applied to examine the effect of magnetic saturation. When a north pole is aligned with the coil (i.e., $\theta_{r0} = 0°$), the magnetomotive force (MMF) of the positive current is in additive direction to the MMF of the rotor magnet. Magnetic saturation then makes the amplitude of positive current higher than that of the negative current. The reverse applies when the magnetic polarity of the rotor changes. Fig. 12(a) shows experimental results of phase current when the

rotor angle was set at $\theta_{r0} = 0°$ and a square-wave ac voltage was applied to the motor. The difference in the amplitudes of positive and negative current peaks is easily observed. Fig. 12(b) shows the results for $\theta_{r0} = \pi$. It is observed that the amplitude of positive current is smaller than that of negative current. From the amplitudes of current, the magnetic polarity of the initial rotor position can be determined.

VI. Conclusion

This paper has investigated some of the major problems associated with the DTC scheme of an IPM motor and their mitigation techniques. The offsets in the sensor outputs of the dc-link voltage and stator current, the stator resistance variation,and requirement of initial rotor position were investigated with the help of modeling and experimental results. The suitability of a three-stage cascaded filter in overcoming offsets in measurements, and of a PI estimator for tracking the stator resistance variation based on the stator currents, were demonstrated. Additionally, the initial rotor position is also identified with sufficient accuracy. All of these remedies enhance the operation of the DTC IPM drive.

References

[1] M. F. Rahman, L. Zhong, W. Y. Hu, K. W. Lim, and M. A. Rahman, "A direct torque controller for permanent magnet synchronous motor drives," *IEEE Trans. Energy Conversion*, vol. 14, pp. 637–642, Sept. 1997.

[2] M. F. Rahman, L. Zhong, and K. W. Lim, "A direct torque controlled interior magnet synchronous motor drive incorporating field weakening," *IEEE Trans. Ind. Applicat.*, vol. 34, pp. 1246–1253, Nov./Dec. 1998.

[3] Y. A. Chapuis, D. Roye, and J. Davoine, "Principles and implementation of direct torque control by stator flux orientation of an induction motor," in *Conf. Rec. IEEE-IAS Annu. Meeting*, vol. 1, 1995, pp. 185–191.

[4] B. K. B. And and N. R. Patel, "A programmable cascaded low-pass filter-based flux synthesis for a stator flux-oriented vector-controlled induction motor drive," *IEEE Trans. Ind. Electron.*, vol. 44, pp. 140–143, Feb. 1997.

[5] P. Vas, *Sensorless Vector and Direct Torque Control*. London, U.K.: Oxford Univ. Press, 1998.

[6] M. R. Zolghadri and D. Roye, "A fully digital sensorless direct torque control system for synchronous machine," *Elect. Mach. Power Syst.*, vol. 26, pp. 709–721, 1998.

[7] S. Mir, M. E. Elbuluk, and D. S. Zinger, "PI and fuzzy estimators for tuning the stator resistance in direct torque control of induction machines," *IEEE Trans. Power Electron.*, vol. 13, pp. 279–287, Mar. 1998.

[8] L. Zhong, M. F. Rahman, K. W. Lim, Y. Hu, and Y. Xu, "A fuzzy observer for induction motor stator resistance for application in direct torque control," in *Conf. Rec. IEEE Power Electronics and Drive Systems Conf.*, 1997, pp. 91–96.

[9] B. S. Lee and R. Krishnam, "Adaptive stator resistance compensator for high performance direct torque controlled induction motor drive," in *Conf. Rec. IEEE-IAS Annu. Meeting*, St. Louis, MO, 1998, pp. 423–423.

[10] M. E. Haque and M. F. Rahman, "Influence of stator resistance variation on direct torque controlled interior permanent magnet synchronous motor drive performance and its compensation," in *Conf. Rec. IEEE-IAS Annu. Meeting*, 2001, pp. 2563–2569.

[11] R. Dhaouadi, N. Mohan, and L. Norum, "Design and implementation of an extended Kalman filter for the state estimation of a permanent magnet synchronous motor," *IEEE Trans. Power Electron.*, vol. 6, no. 3, pp. 491–497, 1991.

[12] M. Schroedl, "Sensorless control of AC machines at low speed and standstill based on the "INFORM" method," in *Conf. Rec. IEEE-IAS Annu. Meeting*, San Diego, CA, Oct. 6–10, 1996, pp. 270–277.

[13] ——, "Sensorless control of permanent magnet synchronous motors," *Elect. Mach. Power Syst.*, vol. 22, no. 2, pp. 173–185, Mar./Apr. 1994.

[14] R. B. Sepe and J. H. Lang, "Real-Time observer-based (Adaptive) control of a permanent-magnet synchronous motor without mechanical sensors," *IEEE Trans Ind. Applicat.*, vol. 28, pp. 1345–1352, Nov./Dec. 1992.

[15] A. B. Kulkarni and M. Ehsani, "A novel position sensor elimination technique for the interior permanent magnet synchronous motor drive," *IEEE Trans. Ind. Applicat.*, vol. 28, pp. 144–150, Jan./Feb. 1992.

[16] S. Ogasawara and H. Akagi, "An approach to real time position estimation at zero and low speed for a PM motor based on saliency," in *Conf. Rec. IEEE-IAS Annu. Meeting*, San Diego, CA, Oct. 6–10, 1996, pp. 29–35.

[17] S. Ostlund and M. Brokemper, "Sensorless rotor-position detection from zero to rated speed for an integrated PM synchronous motor drive," *IEEE Trans. Ind. Applicat.*, vol. 32, pp. 1158–1165, Sept./Oct. 1996.

[18] P. B. Schmidt, M. L. Gasperi, G. Ray, and A. H. Wijenayake, "Initial rotor angle detection of a nonsalient pole permanent magnet synchronous machine," in *Conf. Rec. IEEE-IAS Annu. Meeting*, New Orleans, LA, Oct. 5–9, 1997, pp. 549–463.

[19] T. Noguchi, K. Yamada, S. Kondo, and I. Takahashi, "Initial rotor position estimation method of sensorless PM motor with no sensitivity to armature resistance," *IEEE Trans. Ind. Electron.*, vol. 45, pp. 118–125, Feb. 1998.

[20] M. W. Degner and R. D. Lorenz, "Using multiple saliencies for the estimation of flux, position, and velocity in AC machines," in *Conf. Rec. IEEE-IAS Annu. Meeting*, New Orleans, LA, Oct. 5–9, 1997, pp. 760–767.

[21] M. J. Corley and R. D. Lorenz, "Rotor position and velocity estimation for a salient-pole permanent magnet synchronous machine at standstill and high speeds," *IEEE Trans. Ind. Applicat.*, vol. 34, pp. 784–789, July/Aug. 1998.

[22] A. Consoli, G. Scarcella, and A. Testa, "Sensorless control of AC motors at zero speed," in *Proc. IEEE ISIE*, vol. 1, Bled, Slovenia, July 1999, pp. 373–379.

[23] M. E. Haque, L. Zhong, and M. F. Rahman, "The effect of offset error and its compensation for a direct torque controlled interior permanent magnet synchronous motor drive," in *Proc. IEEE Electric Machines and Drives Conf. (IEMDC'01)*, Cambridge, MA, June 17–20, 2001, pp. 814–819.

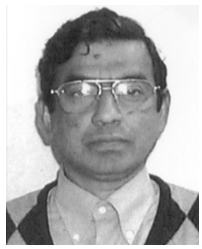

Muhammed Fazlur Rahman (M'79–SM'96) graduated in electrical engineering from Bangladesh University of Engineering and Technology, Dhaka, Bangladesh, in 1972, and received the Masters and Ph.D. degrees from the University of Manchester, Manchester, U.K., in 1975 and 1978, respectively.

He was a Systems Design Engineer with the General Electric Projects Company, Rugby, U.K., for two years before joining the National University of Singapore in 1980. In 1988, he joined The University of New South Wales, Sydney, Australia, as a Senior Lecturer. He is currently an Associate Professor. His research interests are power electronics, motor drives, electrical machines, and motion control systems.

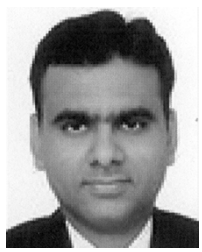

Md. Enamul Haque (M'97) was born in Bangladesh in 1970. He graduated in electrical and electronic engineering from Bangladesh Institute of Technology, Rajshahi, Bangladesh, in 1995, received the M.Engg. degree in electrical engineering from University Technology Malaysia, Johor Bahru, Malaysia, in 1998, and received the Ph.D. degree in electrical engineering from The University of New South Wales, Sydney, Australia, in 2002.

He is currently an Assistant Professor in the Department of Electrical Engineering, King Saud University, Riyadh, Saudi Arabia. His research interests are in electronics, power electronics, and computer control of ac motor drives.

Lixin Tang (S'00) received the B.Eng. and M.Eng. degrees in electrical engineering from Nanjing University of Aeronautics and Astronautics, Nanjing, China, in 1991 and 1994, respectively. He is currently working toward the Ph.D. degree in electrical engineering at The University of New South Wales (UNSW), Sydney, Australia.

From April 1994 to August 1998, he was with the Beijing Institute of Mechanical Equipment, first as an Assistant Electrical Engineer, and then, from 1996, as an Electrical Engineer. He participated in several projects on static frequency converters. In August 1998, he joined GE Hangwei Medical Systems Company Ltd. as a Senior Electrical Engineer, where he was in charge of the redesign, quality control, and technical support of the X-ray generator (XG) subsystem of several CT scanners. He is currently a part-time Teaching Assistant at UNSW. His research interests are ac drives and power converters.

Limin Zhong received the B.E. degree in electronic engineering from Zhejiang University of Technology, Hangzhou, China, in 1985, and the M.E. and Ph.D. degrees in electrical engineering from The University of New South Wales, Sydney, Australia, in 1994 and 1999, respectively.

From 1985 to 1992, he was a Design Engineer with Hangzhou Research Institute of Electrical Machine Drives, China. From 1997 to 2001, he was an Electronics Design Engineer with Legrand Australia. Currently, he is an Electrical Engineer with Cochlear Limited, Lane Cove, Australia. His research interests are in power electronics and motor control.